

Article

Study on Siphon Drainage Capacity of Slopes with Long-Horizontal Pipe Sections

Yingqiu Zhang ¹, Hongyue Sun ² and Yuequan Shang ^{1,*}¹ Department of Civil Engineering, Zhejiang University, Hangzhou 310058, China² Ocean College, Zhejiang University, Zhoushan 316021, China

* Correspondence: syq@zju.edu.cn

Abstract: Siphon drainage, which is applicable in engineering as one of the effective methods to maintain slope stability, has many advantages, including no additional power requirements, simple construction, and low construction cost. However, due to topographic constraints and high farmland occupation costs, most projects inevitably use pipes with a total length of more than 100 m and horizontal sections of more than 50 m for drainage. The increase in pipe length has serious adverse effects on the siphon drainage process, limiting its drainage capacity and long-term applicability. Therefore, in slope siphon drainage, drainage efficiency and long-term effectiveness are critical factors in determining whether a particular pipe size can be used effectively for slope drainage management. This paper investigates the performance of different pipe diameters in drainage capacity, flow regime, and restarting ability under different head and pipe length combinations through theoretical analysis and extensive foot-scale model tests. It was found that a 5 mm pipe diameter, as a transitional pipe diameter between capillary and typical pipe diameter, has both capillary and gravity-dominated characteristics under different capillary and Reynolds number conditions, which can form a stable segmental plug flow while maintaining the presence of liquid film and preventing increased frictional losses along the course.

Keywords: siphon drainage; slug flow; drainage capacity; long-distance horizontal section



Citation: Zhang, Y.; Sun, H.; Shang, Y. Study on Siphon Drainage Capacity of Slopes with Long-Horizontal Pipe Sections. *Appl. Sci.* **2022**, *12*, 9650. <https://doi.org/10.3390/app12199650>

Academic Editor: Filippo Berto

Received: 27 August 2022

Accepted: 9 September 2022

Published: 26 September 2022

Publisher's Note: MDPI stays neutral with regard to jurisdictional claims in published maps and institutional affiliations.



Copyright: © 2022 by the authors. Licensee MDPI, Basel, Switzerland. This article is an open access article distributed under the terms and conditions of the Creative Commons Attribution (CC BY) license (<https://creativecommons.org/licenses/by/4.0/>).

1. Introduction

Landslide disasters mainly occur in the rainy season, related to the softening of slope soils, reducing shear strength, and increasing pore water pressure caused by increased groundwater levels due to rainfall [1,2]. Therefore, timely reduction of the groundwater level is the most direct and effective control method with low cost [3], on consideration of the disaster-causing factors. Siphon drainage technology has remarkable advantages among the various methods to reduce the groundwater level. The siphon drainage method for slopes uses active suction and discharge of deeply buried groundwater from the slope by the siphon phenomenon under the action of atmospheric pressure difference, which means that the technology does not require additional continuous energy supply, as shown in Figure 1. In other words, siphon drainage technology requires no post-maintenance, which helps to reduce the overall project budget [4]. In addition, compared to traditional drainage methods such as horizontal drainage boreholes and surface drainage, siphon drainage technology is simple and very inexpensive to construct, requiring only boreholes for the slope and the placement of siphons in them; once the construction plan is selected, it can be constructed quickly to cope with the upcoming extreme rainfall [5]. Therefore, the initial drainage effect can meet or exceed the standard requirements during the preliminary engineering phase of siphon drainage technology application [6].

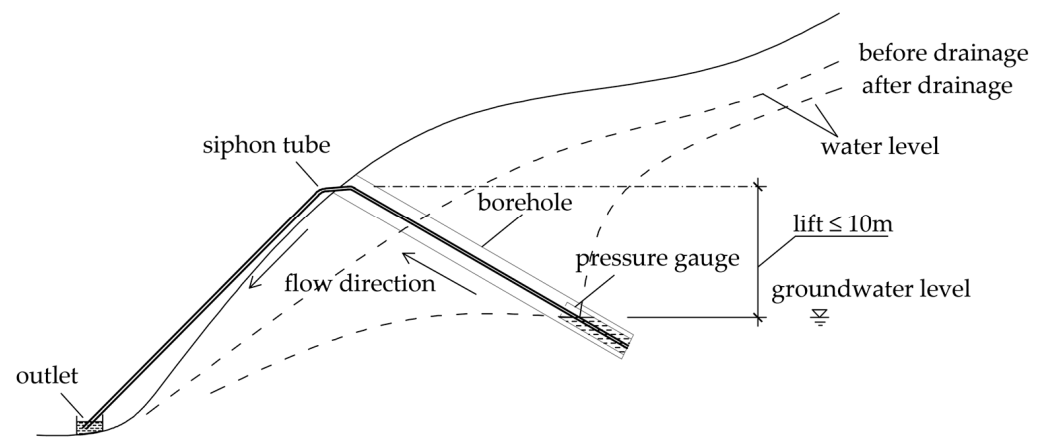


Figure 1. Schematic diagram of inclined pipe siphon drainage method.

However, several studies and engineering practices have shown that the long-term effectiveness of siphoning still faces significant technical challenges [7–11] because slope siphon drainage technology still has drawbacks that limit its overall development. Most landslide treatment projects inevitably require using pipes with a total length of more than 100 m and horizontal sections longer than 50 m for drainage due to topographic constraints and increased economic costs due to farmland occupation, as shown in Figure 2. This increase in pipe length has serious adverse effects on the siphon drainage process. First, the siphon limit lift is significantly reduced, while the drainage capacity is limited when approaching the limit lift. The siphon discharge capacity changes dynamically depending on the water level. When the groundwater level is high, the siphon lift is small, and the siphon will have a high discharge power; conversely, when the groundwater level drops, the siphon head increases, and the siphon discharge capacity decreases. The local atmospheric pressure determines the value of the ultimate head of the siphon. If we ignore the along-range and local head losses generated by fluid flow in the pipe, the ultimate siphon head is the height of the water column equivalent to the local atmospheric pressure. Therefore, the drainage capacity of the siphon is further limited by the resistance of the siphon to the fluid. In addition, after a long dry season, it is difficult to restart siphon drainage during the rainy season when the groundwater level rises again, and the phenomenon of “breakage” tends to occur due to the accumulation of air bubbles at the top of the pipe, which occurs when the siphon stops flowing for a long time due to a variety of factors. The accumulation of air leads to the destruction of the vacuum characteristics at the top of the pipe, which eventually reduces the restarting ability of the siphon and even renders the siphon device useless. The increased difficulty of siphon restart after dry season drainage stagnation limits its long-term effectiveness and reduces the safety of landslide management projects. According to a study by Cai et al. [7], reducing the pipe diameter to form a segmental slug flow can timely discharge the air bubbles from the pipe and prevent air accumulation during the siphoning action. However, the existing 4 mm pipe diameter has a small drainage capacity in protection projects with high water tables or large landslide volumes. Therefore, it is necessary to increase the borehole density, which dramatically increases the project cost and engineering complexity. On the other hand, increasing the drainage pipe diameter may cause air to accumulate in the pipe, reducing the “negative pressure” in the pipe to maintain the siphon operation and eventually leading to severe consequences of siphon failure.

In summary, the complex engineering conditions place higher demands on the promotion of small-diameter siphon drainage technology for sloping surfaces, i.e., to meet short-term rapid drainage while meeting effective long-term operation. Combining the findings of the Cai study on siphon diameter, this paper investigates the selection of pipe diameter in siphon technology through theoretical analysis and foot-scale model tests. With

the characteristics of the gas-liquid two-phase flow in the pipe and the wall effect considered, the optimal pipe diameter for siphon drainage technology can be further explored.

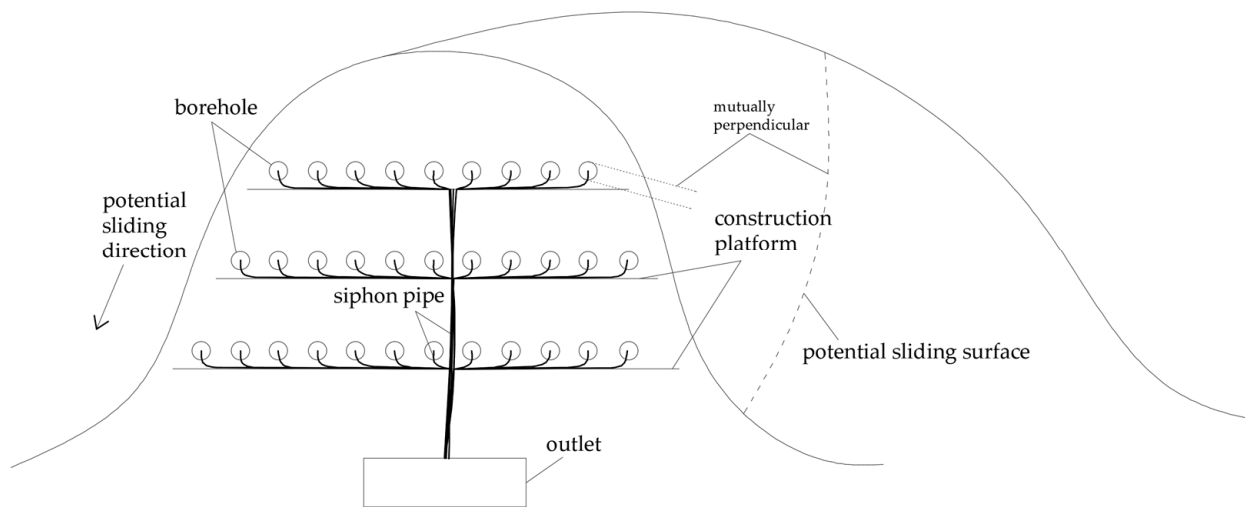


Figure 2. Schematic diagram of the inclined pipe siphon drainage method with long horizontal pipe sections (front view).

2. Siphon Drainage Test

2.1. Test Model Setup and Scheme

In order to study the variation in the efficiency of the slope siphon drainage system under the dual effect of pipe length and pipe diameter, several sets of controlled experiments were conducted to select the most suitable siphon pipe diameter for the engineering scenario by comparing the evaluation factors such as the working flow rate, the flow pattern in the pipe, and the restarting capacity of the siphon drainage system.

The siphoning phenomenon is triggered by an entire tube of liquid under the effect of water head difference, which in turn is maintained under pressure difference between atmospheric pressure and negative pressure inside the tube, i.e., ambient air pressure is an essential factor affecting the siphoning characteristics. Further, the reduction of pipe diameter and length in the reduced size model also requires a proportional change in the test ambient air pressure and liquid properties. Therefore, in order to reduce test errors, the experimental setup uses a full-size model with pipes made of polyurethane (PU).

The siphon drainage experimental set-up, as shown in Figure 3, was used to validate the proposed calculation method. The whole model is a complete siphon system, consisting of a constant lift water supply device, a siphon pipe (partitioned into rising fluid section, fluid horizontal movement section, and fluid falling section according to the function and fluid force characteristics), a constant lift water storage device, and a scale. The storage barrel set at the bottom of the rising fluid section of the siphon (later referred to as the rising section, horizontal section, and falling section) simulates the change of the groundwater level at the bottom of the borehole in different seasons of the actual project, and the change range is 3–12 m. The water storage bucket is a fixed-position constant lift device, and the height of the water surface in the bucket from the top of the siphon (horizontal section) is 17.2 m.

The siphoning action starts when the siphon tube connecting the upper and lower water levels is filled with fluid, and the fluid in the drain tube at the lower water level moves under the action of gravity. The fluid in the inlet pipe then overcomes gravity to follow the flow under the action of intermolecular cohesion and negative pressure at the top, forming a continuous siphon flow, as shown in Figure 4. After the fluid movement in the siphon reaches the state of stable siphoning, the flow monitoring starts. Fifty-two experiments were performed, and the schemes are given in Table 1, where D represents the diameter of siphon pipe, L_{hori} represents the horizontal section length of siphon pipe,

and H represents the siphon lift. The flow velocity was measured by weighting the water collected in the water storage tank for a period. It should be noted that a single-phase flowmeter did not work well in these experiments since the flow pattern is multi-phase. Due to the inhomogeneity and randomness of the gas-liquid two-phase flow in the siphon, we performed repeated measurements until the fluctuation of the siphon flow rate under each condition did not exceed 2%, while the test measurements were obtained by removing the maximum and minimum values and taking the average value. We used the drainage velocity to measure the siphon drainage capacity under the corresponding conditions, while for its long-term applicability, it was evaluated by comparing the restarting capacity after the siphon stopped flowing. The same experimental model was used to simulate this process in this part of the study. The test procedure was as follows: increase the siphon lift above the limit, keep the inlet pipe submerged in the storage tank all the time, and after a resting period, remove the tank and observe the phenomenon; reduce the siphon lift until the siphon process restarts and measure the siphon lift at that moment. In order to facilitate the expression, the unified “D—diameter number” substitutes the specific diameter siphons, i.e., D-5 refers to the 5 mm siphon. In addition, for easier understanding, we specify a high-lift siphon flow when the lift is not less than 7 m.

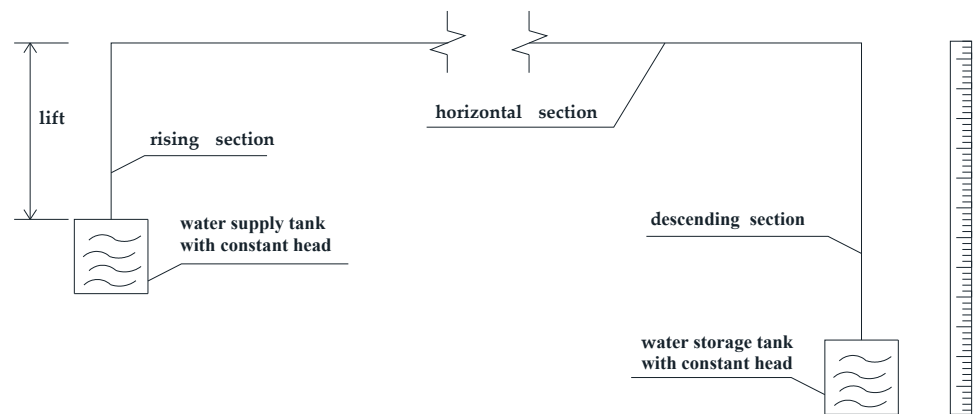


Figure 3. Diagram of the test device.

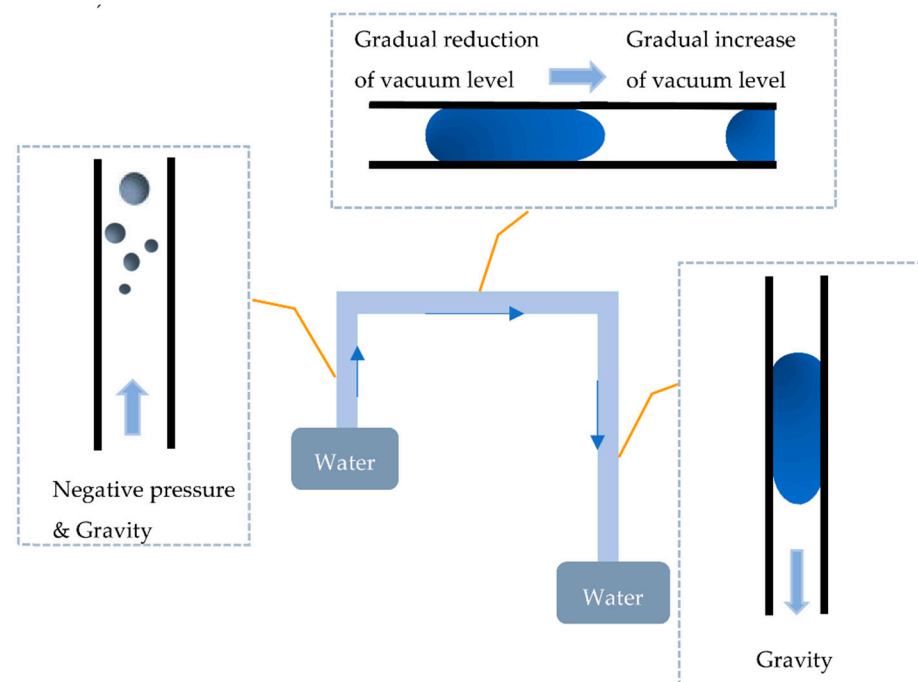


Figure 4. Schematic diagram of the gas phase precipitation mechanism during siphon drainage.

Table 1. Experimental schemes of siphon drainage ($T = 25\text{ }^{\circ}\text{C}$, $P_{la} = 100.53\text{ kPa}$).

No.	D /[mm]	L_{hori} /[m]	H_{lift} /[m]
1–10	3, 4, 5, 6.5, 8	0	3, 5
11–20	3, 4, 5, 6.5, 8	0	7, 8
21–28	3, 4	80, 160	4, 6
29–32	5	80, 160	3, 6
33–40	6.5, 8	80, 160	3, 5
41–44	4	80, 160	7, 8
45–48	5	80, 160	7, 8
48–50	6.5	160	7, 8
51–52	8	160	7, 8

2.2. Siphon Flow Period

During siphon drainage, many flow patterns exist, including bubble flow, bubbling flow, and slug flow. In D-3–5 pipes, slug flow is the dominant flow pattern, while in D-6.5–8 pipes, slug flow and churn flow are both spotted.

The shape and size of the bubbles in the siphon drain's vertical rise section determine the size of the water cross section and the main flow pattern in the horizontal section. The air pressure inside the pipe gradually decreases when the liquid is lifted in the rising section. Henry's law shows that the reduction of air pressure will cause the precipitation of the original dissolved gas in the water if temperature and other environmental factors remain unchanged. Therefore, with the continuous forward motion of the fluid in the siphon tube, the flow is transformed from a single fluid to a gas-liquid two-phase mixed fluid motion. In Schemes 41–50, as the height rises, round bubbles gradually appear and are accompanied by trembling motion, while the tube wall has attached many tiny stationary bubbles. However, in Schemes 51–52, the stationary bubbles gradually evolved into moving spherical and long ellipsoidal bubbles with diameters ranging from 3 to 7 mm as the observed height increased.

In the D-3–4 pipes, the horizontal section of the siphon is mainly in the form of segmental slug flow: the front of the segmental slug bubble is curved with some curvature, and the tail is closer to a flat surface. The type of slug flow in the tube can be further classified as dry slug flow. When the siphon flow in the D-5 pipe enters the horizontal section, the main flow pattern of gas-liquid two-phase flow is mainly wet slug flow, with occasional appearance of dry slug flow. The difference between dry and wet slug flow manifestations is determined by the bubbles, which are composed of only the gas-liquid interface in wet slug flow, while the bubbles in dry slug flow are composed of both gas-liquid interfaces as well as the pipe wall. In horizontal sections of D-6.5–8 pipes, due to the effect of gravity and liquid surface tension, the churn and the slug flow are dominant flow pattern, with bubbles deviating from the midline and adhering to the upper wall of the tubes. In addition, many tiny stationary bubbles can be observed in the D-8 pipe attached to the wall but keep merging with the later moving long bubbles. It should be noted that the bubbles in the D-6.5–8 pipes are irregular and their longitudinal profiles are asymmetric up and down, as shown in Figure 5c,d; while the bubbles in the D-3–5 pipes are more regular in shape and longitudinal profiles are symmetric up and down, as shown in Figure 5a,b.

A sudden acceleration of the fluid can be observed at the junction of the horizontal and vertical descending section: the bubble deformation elongates, and the shape becomes irregular. However, this process lasts only for a short period, and the flow pattern of the vertical section soon returns to the same as that of the horizontal section. The bubbles may merge during the motion but not redissolve in the water. Eventually, the siphon flow will still be discharged from the siphon tube as a gas-liquid two-phase flow.

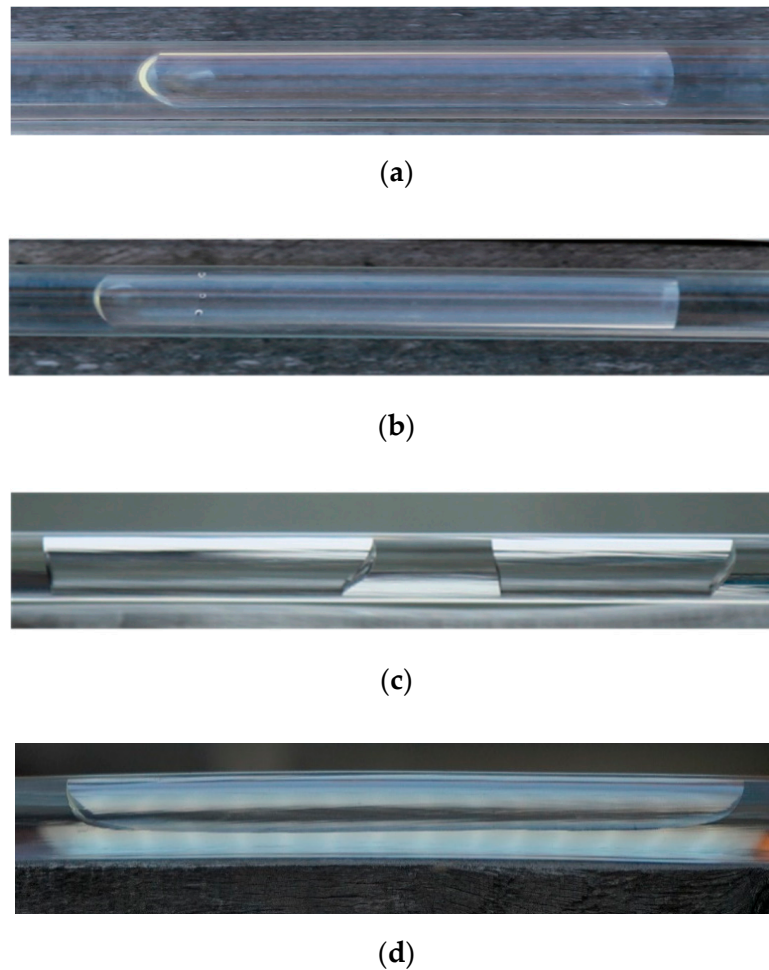


Figure 5. Bubble pattern in the siphon tubes: (a) D-3-4; (b) D-5; (c) D-6.5; (d) D-8.

2.3. Siphon Resting Period and Restart

In the application cycle of the project, the resting and restarting process of the fluid in the pipe in a short siphon drainage system can be simplified to a transient process. In contrast, in a siphon with a horizontal section length of more than 10 m, the rising water level causes a gradual gas-liquid two-phase step-by-step push in the horizontal section, and the duration of this process cannot be ignored. In this pushing process, the rising water level causes an increase in potential energy, converted into kinetic energy, causing fluid movement in the tube. When the end of the horizontal section of the fluid segment passes the horizontal section, gravitational potential energy converts into kinetic energy. The siphoning is completed when the fluid in the horizontal section also moves under the negative pressure generated by the descending fluid motion.

According to the calculation formula of pipe flow movement, the pipe diameter and length are the key factors affecting the reduction rate of restarting lift under the premise that the pipe, fluid composition type, temperature, atmospheric pressure, and other conditions are determined. The siphon lift loss caused by the pipe diameter size is mainly determined by the along-stream loss and air accumulation. The flow rate and pipe diameter are negatively related to the along-stream loss coefficient. Therefore, the smaller the pipe diameter, the larger the along-travel loss coefficient for a stationary fluid in the siphon stopping period. The air accumulation problem is determined by the main flow pattern of the fluid in the siphon.

During the standstill period, many segmental bubbles are observed in the horizontal section of the siphon. The main shape of the bubbles varies with the size of the tube diameter: the segmental bubbles in the D-3-5 pipes are smaller in size, and the gas-liquid

interface at both ends is less affected by gravity, so the upper and lower sides of the bubbles can be considered symmetrical along the central axis of the siphon and form two independent gas-liquid interfaces, as in Figure 6a,b. In the horizontal section of the D-6.5–8 pipes, the presence of segmental bubbles occupying the entire cross-section of the siphon can still be observed, but more floating bubbles replaced the segmental bubbles against the pipe wall. The interface morphology on both sides of the slug bubbles changed significantly: the longitudinal profile of the gas-liquid interface was symmetrical at a point on the central axis of the siphon or was a single curved surface with the wall surface forming upward-facing wall bubbles, as shown in Figure 6c,d.

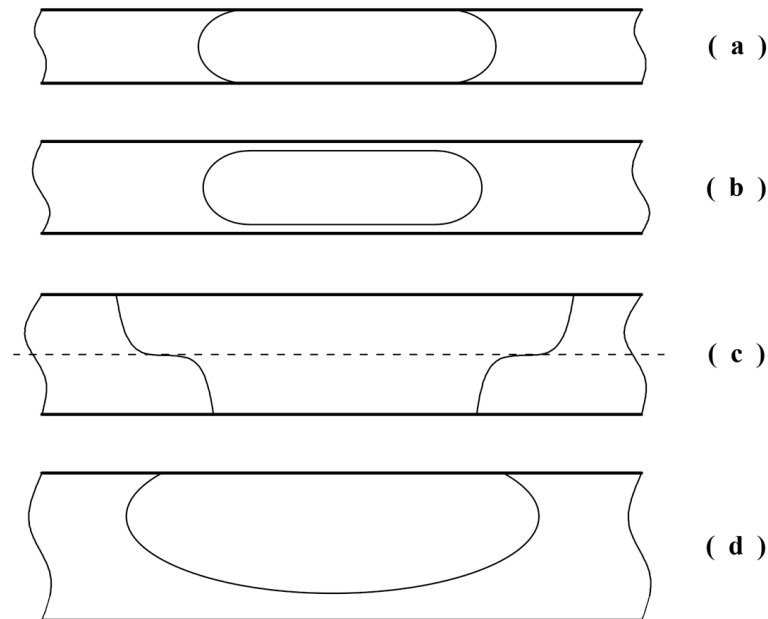


Figure 6. Schematic diagram of gas-liquid interface morphology in longitudinal section of various pipe diameters: (a) D-3–4; (b) D-5; (c) D-6.5; (d) D-8.

When the water supply level rises, the fluid in the rising section of the siphon will then push the fluid in the horizontal section towards the drain. In the D-3–5 pipes, the horizontal section of the fluid undergoes a discontinuous motion under the action of the thrust. In this form of flow, bubbles and liquid velocity are the same, alternating through the pipe and a liquid film on the pipe wall is not formed. According to the simplified model, it is known that the pressure drop of the slug flow can be divided into three parts, namely, the frictional pressure drop of the bubble and fluid movement and the frictional pressure drop generated by the movement of the gas-liquid-solid three-phase contact line. In the D-6.5–8 pipes, the tremendous frictional resistance between the floating bubbles and the tube wall seriously hinders the advance of the fluid. Marine engineering of microbubble resistance reduction technology has also confirmed the existence of “a three-phase gas-liquid-solid wall with attached bubbles and the liquid to make a relative motion” mode [12]. The liquid along the resistance declines when the gas-liquid motion is not synchronized. Cai’s work also confirms that the siphoning action in a large-diameter tube caused the accumulation of air in the horizontal section because of the inability to form a slug flow. The accumulation results in the gradual extension of the gravity flow from the vertical descending section to the horizontal section, which in turn causes the length of the complete tube flow in the horizontal section to decrease gradually, eventually leading to a decrease in the specific gravity of the liquid in the second half of the siphon tube to the point where siphoning cannot be maintained.

When the liquid pushes the bubble at the end of the horizontal section into the vertical descending section, the energy will again be converted from kinetic energy to gravitational

potential energy, and the descending liquid section adds a driving force of movement—negative pressure—to the fluid in the horizontal section of the siphon. At this point, the siphoning action in the long tube completes the restarting process. During the restart process, the energy loss mainly consists of the along resistance of bubbles and the liquid slug, the frictional resistance caused by gas-liquid-solid contact line movement, and heat when bubbles are compressed. Therefore, the siphon cannot be restarted when the water level increases to the limit lift before the stopping period.

3. Formation and Pressure Drop Mechanism of the Moving Contact Line

Young’s equation is proposed based on the ideal surface assumption so that the liquid-solid contact angle has only a static value. Frenkel et al., proposed a theoretical framework of molecular dynamics theory, which views the fluid transport process as a process in which external forces drive the fluid molecules to change their vibrational frequency on the solid surface, i.e., the process of adsorption and desorption of liquid molecules on the solid surface leads to energy dissipation at the microscopic scale. Through this theory, intermolecular friction and moving contact lines are effectively linked.

When the three-phase contact line starts to move, the value of pressure drop due to contact angle hysteresis remains constant, but the friction loss of the moving contact line increases continuously due to the effect of velocity on the forward and backward contact angles. The most widely used theoretical models on the relationship between contact angle and contact line velocity are fluid dynamics and molecular dynamics theories [13]. The fluid dynamics theory emphasizes the viscous flow energy dissipation in the triangular region near the contact line. The model is based on the fine-scale (between macroscopic and microscopic) simulation of the gas-liquid-solid three-phase contact line before the continuum rupture, and the interface beyond the contact line is simulated and calculated at the macroscopic scale, as shown in Figure 7. The model requires two empirical parameters to define the fine-scale region, which is macroscopic characteristic length L_{ma} and microscopic characteristic length L_{mi} ; then, we can get

$$\theta_D^3 - \theta_S^3 = 9 \frac{\mu U}{\sigma} \ln \left(\frac{L_{ma}}{L_{mi}} \right) \tag{1}$$

where, μ refers to the water viscosity, σ refers to the surface tension, U refers to the flow velocity, θ_D and θ_S are the dynamic and static contact angles, respectively. The static contact angle reflects the interfacial tension of the material itself, while the dynamic contact angle is the interfacial infiltration angle in a non-equilibrium state. When near-static contact occurs between gas-liquid-solid phases, the surface structure of their materials is the most critical factor in determining the size of the liquid-solid indirect contact angle. However, for a flowing liquid in a circular tube, the dynamic contact angle, which is directly influenced by the flow velocity, is the crucial parameter that really determines the flow pattern.

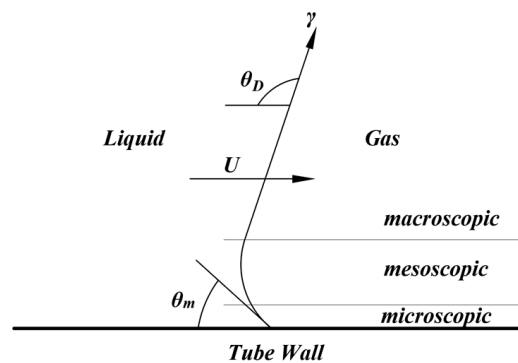


Figure 7. Schematic diagram of microscopic to the macroscopic scale of viscous liquid bending.

On the other hand, molecular dynamics theoretical models suggest that the motion of the contact line is determined by the statistical dynamics of molecular collisions between molecules of gases, solids, and liquids in a three-phase region [14], as defined by the following equation

$$U = 2\kappa^0 \vartheta \sinh \left[\frac{\sigma(\cos \theta_S - \cos \theta_D) \vartheta^2}{2k_B T} \right] \quad (2)$$

where ϑ is the average displacement length, k_B is Boltzmann's constant, h is Planck's constant, T is temperature; κ^0 is the equilibrium frequency of random displacement of molecules, which can be expressed in terms of the activation energy of the wetting process

$$\kappa^0 = \left(\frac{k_B}{h} \right) \exp \left(- \frac{\Delta E}{N k_B T} \right) \quad (3)$$

where, N is Avogadro's constant, ΔE refers to the activation energy.

4. Discussion

4.1. Comparison of Siphon Flow Rates

The siphon drainage rate is directly related to the efficiency of rescue and relief in engineering practice and provides a reference basis for long-term effective groundwater level reduction and maintenance on slopes. Therefore, the siphon drainage rate under different lift, pipe length, and pipe diameter conditions is also vital to improve its engineering applicability.

Lift is one of the fundamental influencing factors of a siphon system, which directly affects the drainage performance of the siphon, as shown in Figure 8a,b. In the legend, the number before the short line represents the siphon diameter, and the number after the short line represents the total length of the siphon. The intersection of the curves with the x-axis is the siphon limit lift for the corresponding conditions. In general, the influence of pipe diameter on the trend of siphon velocity change with a lift is small, and the curves of lift velocity for different pipe diameters show similar trends. From the graphs, the following observations can be made: (1) as the lift increases, the absolute value of the slope of the curve increases, which confirms the principle that the formation of dry plug flow causes high pressure drop under low capillary number conditions; (2) for short siphons, the limit value of the lift increases with the increase of the pipe diameter, but in siphons with long horizontal sections, this law no longer appears. These phenomena are caused by the differences in the manifestations of the slug flow in siphons of different diameters. First, the fluid has enough space and time to form a fully developed slug flow in a siphon with a long horizontal section. Second, the effects of gravity and surface tension in different pipe diameters have different percentages of the effect, as shown by the fact that the smaller the pipe diameter, the more pronounced the effect of surface tension; the more effective the pipe diameter, the more pronounced the effect of gravity. Returning to the problem discussed earlier, in D-3-4 tubes, fluid surface tension plays a dominant role, and bubbles form a symmetrical structure in the tube and form a gas-liquid-solid three-phase moving contact line. The adverse effects of moving contact lines on pressure transfer have been discussed in the previous section, and this is a problem we should try to avoid in our engineering design. Due to the unique dimensions of the D-5 tube, between the capillary tube and standard diameter tube, it possesses transitional characteristics: the tube can form both wet plug flow and ensure that bubbles form a regular shape inside the tube. In the D-6.5-8 tube, gravity plays a dominant role, which leads to bubbles floating up against the wall, while the liquid is mainly distributed in the lower part of the tube. The bubble floating phenomenon will cause an uneven force of fluid in the tube, leading to the phenomenon of "liquid discharge and gas accumulation in the tube". When the gas in the pipe accumulates to a certain level, the siphon will fail.

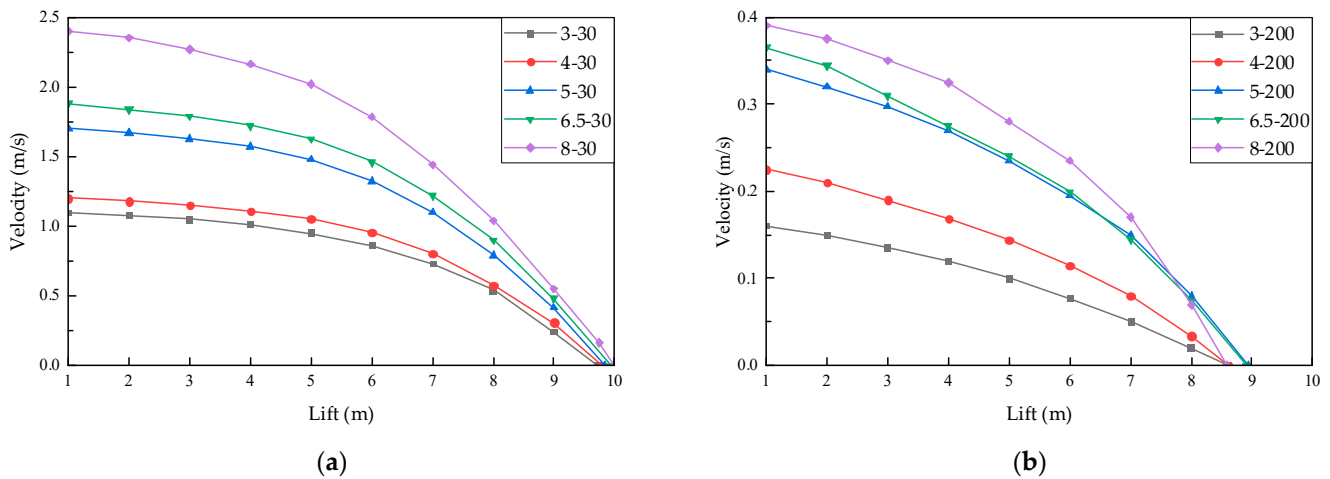


Figure 8. Siphon lift—flow velocity curve: (a) Total length of 30m; (b) Total length of 200m.

4.2. Comprehensive Analysis of Horizontal Section Flow Pattern

Figure 9 shows the flow patterns obtained for different conditions of siphon drainage, where the apparent velocity of the gas phase and the average flow velocity are obtained from experimental measurements. In these plots, the flow patterns of bubble flow ([DB], [B]), intermittent flow ([I], [S]), and annular flow ([A]) within the horizontal section of each siphon with diameters of 3 mm, 5 mm, 6.5 mm, and 8 mm are shown and plotted simultaneously on the flow pattern diagram in the same flow direction to examine the effect of tube diameter on the flow pattern.

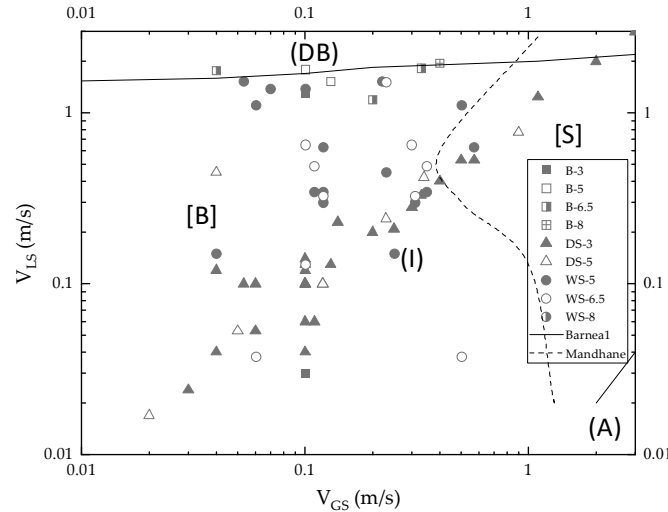


Figure 9. The flow pattern of gas-liquid two-phase in a horizontal circular tube.

The crossed line areas on the map show the areas of bubble flow and annular flow. It is worth noting that the tube diameter has almost no effect on the flow pattern in the range of 3 to 5 mm for this experiment. Figure 9 shows the flow pattern distribution for the horizontal flow of gas-liquid two-phase, and the solid line in the figure shows the gas-liquid two-phase flow pattern boundary obtained by Barnea et al. [15] regarding the diameter of 4 mm, while the dashed line shows the results of Mandhane et al. [16]. In the legend, the letter before the short line represents the abbreviation of the flow pattern, and the number after the short line represents the diameter of the tube, where “B” refers to bubble flow, “DS” refers to dry slug flow, and “WS” refers to the wet slug flow. Figure 9 shows that the data obtained by experiment for D-3–5 tubes can fit well with the flow pattern line of Barnea et al. while the data for D-6.5–8 tubes do not give a good fit. In general, the effect of

tube diameter on the flow pattern is less than that of the data for larger tube diameters in the range of tube diameters tested in this section. According to the test results, the effect brought about by the tube diameter gradually becomes evident when the tube diameter is significantly more than 6 mm. The test results are very similar to the results of flow pattern analysis in the vertical direction by Barnea et al., except that the annular flow region plotted in this test is more comprehensive than that in other cases. This fact suggests that the flow direction does not seriously affect the flow pattern in small diameter tubes.

Analyzed in terms of physical properties, this means that for gas-liquid two-phase flows in circular tubes with diameters no larger than about 5 mm, surface tension has a much more significant effect on the flow pattern than gravity. This argument is also argued in the next section.

4.3. Critical Lift Variation at Siphon Restart

The limiting lift for each pipe diameter before and after the stop flow period is shown in Figure 10. The restarting lift loss rate of the siphon visually reflects the siphon restarting capacity and rain and dry season sustainability for that pipe diameter and length. The siphon restarting capacity of the short pipe siphon is much larger than that of the long pipe siphon: the loss rate along the length of the short pipe siphon is about 1% to 3.5% for the 30–50 m pipe siphon, about 12% to 22% for the 100 m pipe siphon, while the distribution of the 200 m pipe siphon loss rate shows a significant variance of about 15% to 31%. For smaller pipe diameters of 3 to 5 mm, the maximum loss rate of siphon restart lift does not exceed 20%, while for larger diameters, especially for 8 mm siphons, the siphon restart critical lift fluctuation is more significant. While the lift reduction rate for short 8 mm diameter pipes does not exceed 4%, the lift reduction rate for long pipes increases to 19–30%, with a risk of failure.

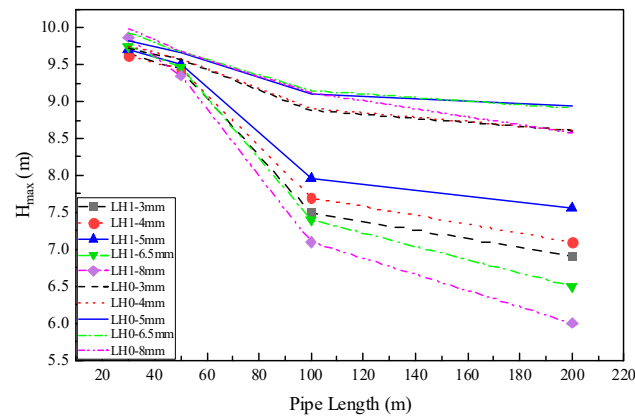


Figure 10. Average initial limit lift and restart limit lift change.

Many experimental studies have shown that the static contact angle is a dynamic value with a range of variation, known as contact angle hysteresis [17–19]. The upper limit of the static contact angle is called the static forward contact angle, while the lower limit is called the static backward contact angle. As the name implies, the static forward contact angle is the contact angle between the liquid and the solid when the liquid phase advances (the front end of the forward direction of the liquid slug), while the static backward contact angle is the contact angle between the liquid and the solid when the liquid phase retreats (the back end of the forward direction of the liquid slug). The dynamic change in the static contact angle caused by the contact angle hysteresis means there may be pressure loss in the fluid in the tube even before the movement starts. When the liquid slug is in the critical state of static-moving, the dynamic advancing and retreating contact angles take the values of static advancing and retreating contact angles, respectively. At this point, the pressure drop caused by the contact angle hysteresis is the maximum of the pressure drop caused

by the static contact line. Taking the concept of contact angle hysteresis into consideration explains well the drop in critical lift during siphon restart.

The test results show that the average length of slug bubbles in the horizontal section of the long-distance siphon drain increases with pipe diameter, as shown in Figure 11. In the horizontal section of D-3–5 pipes, there is no direct rule of slug bubble length with pipe diameter, but the statistical results of D-5 and D-6.5 have evident values of jump variation difference. Combining the statistical values of bubble lengths in the five pipe diameter horizontal sections shows that the average bubble length increases with the increase of pipe diameter when the pipe diameter exceeds 5 mm. In addition, the dispersion of the bubble length distribution is also correlated with the tube diameter, i.e., the dispersion increases positively with the tube diameter. The average bubble length in the horizontal section of the siphon was more considerable for the 6.5 mm and 8 mm diameters compared to the bubble length in the tube with diameters below 5 mm, and no bubbles were observed in the vertical section of the siphon during the standstill period. This is because the bubbles in the vertical section of the siphon move to the horizontal section under buoyancy, which pushes the bubbles in front of them to move further and merge with them to form longer bubbles. The fusion tendency occurs when the distance between bubbles in the same phase is small [20], and the comparison results of the average length of bubbles in the tube before and after the stopping period (change value curve) confirm this idea. In addition, the increase in the average bubble length with the tube diameter can be seen in Figure 11a,b since the resistance to motion of the bubbles decreases with the increase in the tube diameter. When the bubbles are subjected to the thrust generated by the fluid motion in the vertical section, the slug bubbles will move and push the movement of the liquid slug, while the upward floating wall bubbles will remain stationary or move slowly and merge with the slug bubbles.

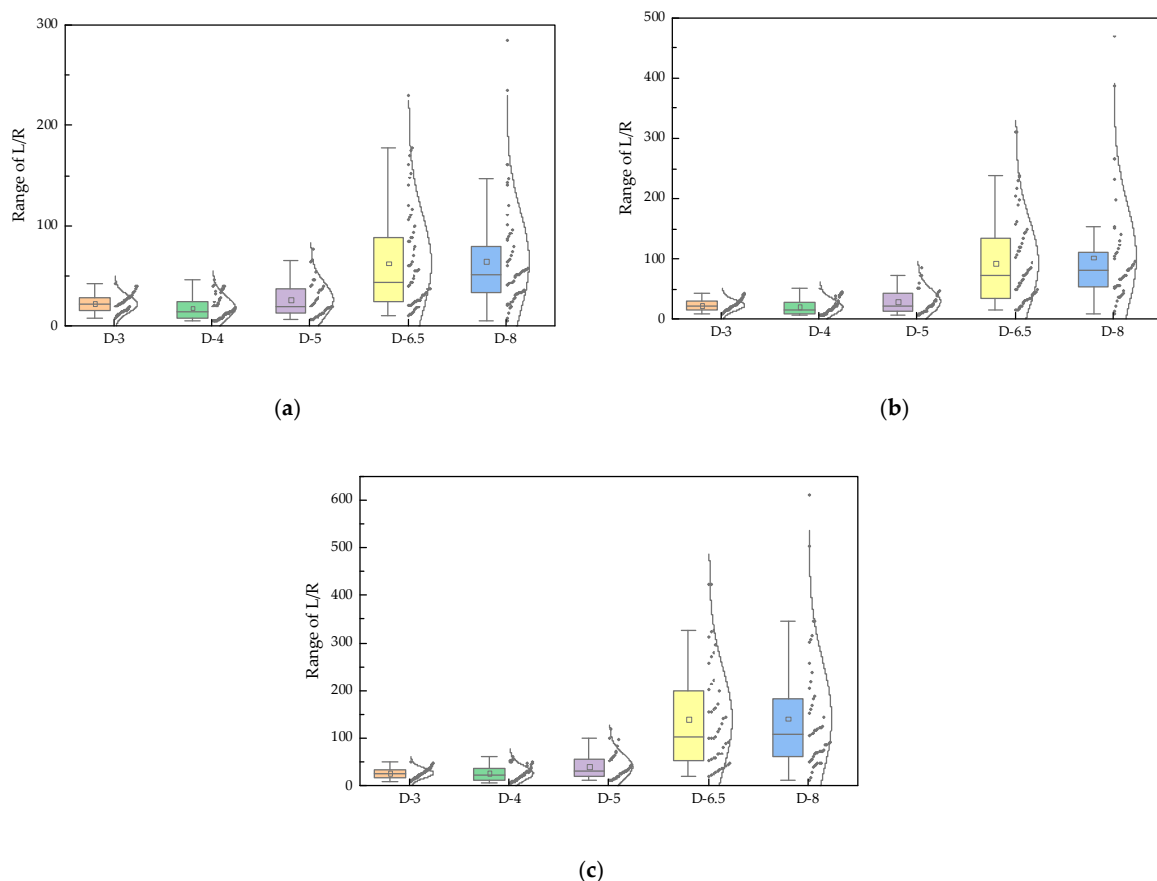


Figure 11. Distribution of bubble lengths in the horizontal section of a long-distance siphon drain: (a) low Ca flow; (b) early stationary phase; (c) late stationary phase.

The main hydrodynamic characteristic behaviors of gas-liquid two-phase flow originate from viscous forces, inertial forces, interfacial forces, and gravity. When the scale range changes, the effects of the different forces become entirely different. While gravity plays a significant role in defining the flow characteristics at conventional sizes, it tends to be negligible at the millimeter/micron scale, and interfacial forces play a more prominent role. Using the Eötvös number, it is possible to set a boundary criterion between these two scales [21,22]. By definition, it can be used to quantify the equilibrium relationship between gravity and interfacial forces.

This is the hydrodynamic phenomenon reflected by the Eötvös number as the relevant characteristic number, and the defined equation is shown below.

$$E\ddot{o} = \frac{g(\rho_L - \rho_G)D^2}{\sigma} \quad (4)$$

where g is the acceleration of gravity, ρ_L and ρ_G are the liquid density and gas density, respectively, D is the tube diameter, and σ is the surface tension.

Removing the catchment tank before the end of the stop-flow period can compare the ability of different diameter siphons to retain water. The results showed that none of the D-3–5 tubes were affected when one end of the tube was not submerged in water, while water occasionally flowed out of the D-6.5 tube and almost all of the D-8 tube failed to retain water. In siphons with diameters no larger than 5 mm, surface tension plays a significant role due to the wall effect. Surface tension forms a gas-liquid-solid three-phase contact line or a gas-liquid two-phase contact surface through wall adhesion, which generates additional pressure more significant than the effect of gravity and forms a curved moon-shaped gas-liquid interface, where the central axis of the interface is parallel to the axis of the tube or forms a slight angle. In large-diameter siphons, the effect of gravity is dominant, and the liquid squeezes the bubbles in the horizontal tube to float upward and form a closed cavity with the tube wall. Similarly, the vertical section of the siphon tube has gas precipitated in the liquid due to changes in air pressure to form bubbles. The bubble movement in the small-diameter circular tube is mainly dependent on the buoyancy and the wall resistance, and before reaching a critical value to slip, the interaction force between the liquid and solid having exponential growth, which can be analogous to the principle of maximum static friction between adjacent solids. Correspondingly, the buoyancy effect on the middle section of the large-diameter circular tube slug bubble is much more significant than the surface tension and the frictional resistance of the three-phase contact line. Hence, the bubble converges to the highest horizontal section under the effect of buoyancy. Under the combined effect of the above conditions, the bubble length statistics are formed, as shown in Figure 11.

4.4. Calculation of Slope Drainage Capacity Requirements in Combination with Single-Hole Gushing Water

In order to improve the applicability of slope siphon drainage methods in actual projects, a reasonable arrangement of siphon drainage hole clusters is required to improve the efficiency of lowering the groundwater table, which requires quantifying the slope drainage requirements and the drainage volume of siphon boreholes.

The French scholar Dupuit proposed his famous steady well flow equation. He proposed the idea of the round island model: in a homogeneous, isotropic, submerged aquifer with a horizontal water barrier floor, with a complete well as the center and a constant head on the outside, without precipitation infiltration recharge and groundwater evaporation, the seepage flow is stable. Then, the flow rate or drop depth for a fixed value of water pumping from the well is controlled and at a particular time, seepage will reach a steady state, aquifer diving surface from the horizontal surface to funnel-shaped—Dupuit called it a water level landing funnel.

According to the principle of seepage continuity, the cross-sectional flow within the radius of the influence of the pumping well is equal to the flow of the pumping well. Dupuit

well flow is radial flow, and the hydraulic gradient at each point decreases as the distance between that point and the wellbore increases, while the hydraulic gradient is greatest near the well bore. The flow line near the bottom plate of the water barrier is straight, and the infiltration curve is convex, i.e., the flow line gradually transitions from a convex curve on the diving surface to a straight line. The iso-head surface in the well flow model is a series of surfaces formed by the rotation of the iso-head line on the profile around the well axis. In order to obtain these complex surface equations, Qubuyi ignores the flow velocity in the vertical direction and approximates the iso-head line on the profile as a plumb line, which reduces the three-dimensional well flow problem to a two-dimensional flow problem.

The water barrier floor is used as the reference surface for the derivation of the equation, and the head value at the diving surface is equal to the seepage thickness h . According to the polar axis, the well axis is taken as the h (seepage thickness) axis, which is positive upward; the r axis is taken along the water barrier floor, which is positive outward, as shown in Figure 12.

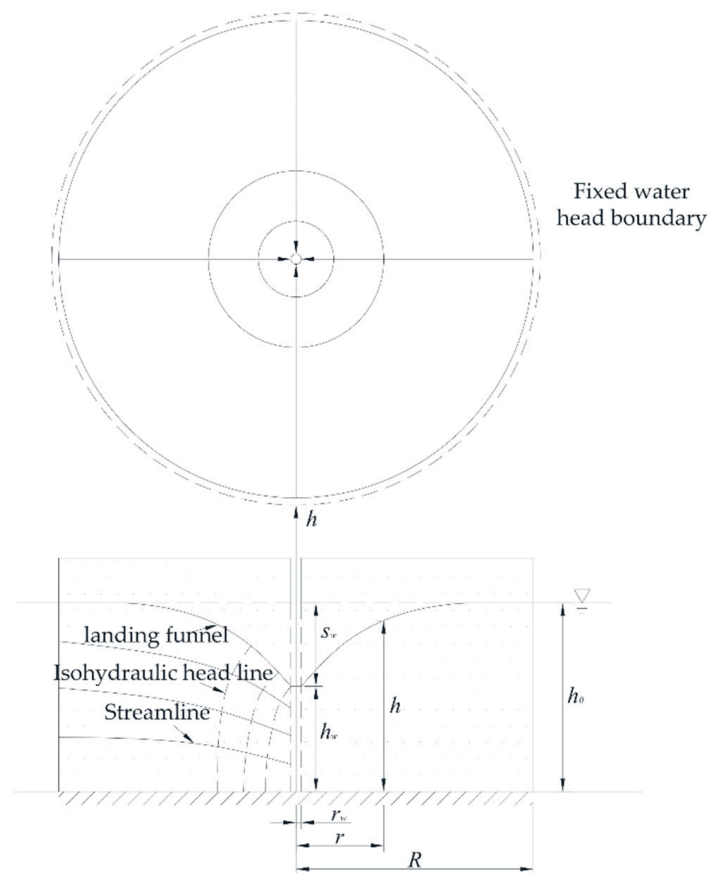


Figure 12. Schematic of Dupuit stabilized submerged well flow.

According to Darcy’s law and Dupuit’s assumption, the flow rate of an arbitrary seepage cross section is as follows:

$$Q_0 = KA \frac{dh}{dr} \tag{5}$$

Since h increases with r , and thus $\frac{dh}{dr} > 0$, considering the seepage section as a cylindrical surface, so $A = 2\pi rh$, then

$$Q_0 = 2\pi rhK \frac{dh}{dr} \tag{6}$$

Integrate over r and h , respectively, where r is from r_w to R ; h is from h_w to h_0 . According to the formula of the surging volume of Dupuit stabilized submerged well flow, it is known that.

$$Q_0 = \pi K \frac{h_0^2 - h_w^2}{\ln \frac{R}{r_w}} \tag{7}$$

where Q_0 is the pumping flow rate, h_0 is the water level (from the water barrier bottom) or seepage thickness at the outer boundary of the water content, h_w is the water level (from the water barrier bottom) or water layer thickness in the well, R is the radius of the cylindrical aquifer, r_w is the radius of the well, and K is the aquifer permeability coefficient.

Wu [23] used this formula to analyze and calculate the single-hole seepage volume, combining the good cluster hole precipitation capacity with the siphon inclined hole drainage capacity and introducing the concept of drainage interception ratio. According to Wu’s research results, this can be directly calculated to obtain the single-hole water influx, as shown in Table 2.

Table 2. Single borehole gushing capacity.

Permeability Coefficient	Gushing Capacity			
	Groundwater Level Drop at the Borehole Bottom (s_w)			
	5 m	10 m	15 m	20 m
10^{-3} cm/s	11.27	38.44	79.64	134.05
10^{-4} cm/s	1.39	4.59	9.37	15.62
10^{-5} cm/s	0.18	0.57	1.14	1.87
10^{-6} cm/s	0.03	0.08	0.14	0.23

For slopes, controlling the groundwater level in the slope body below the danger level of the landslide is the primary condition to be met by the drainage system. Therefore, the drainage capacity of the siphon drainage hole needs to meet the condition that when heavy rainfall occurs, the groundwater level caused by the infiltration of rainfall into the slope body cannot exceed the controlled groundwater level after it rises. The amount of rainfall infiltration is related to many complex factors such as topographic conditions, climatic environment, slope size, and geotechnical structure, etc., and cannot be fully quantified for analysis. However, the maximum amount of groundwater infiltration on slopes will not exceed the amount of infiltration when the water table reaches the slope surface. The siphon discharge volume can be calculated from the siphon discharge rate according to the following equation.

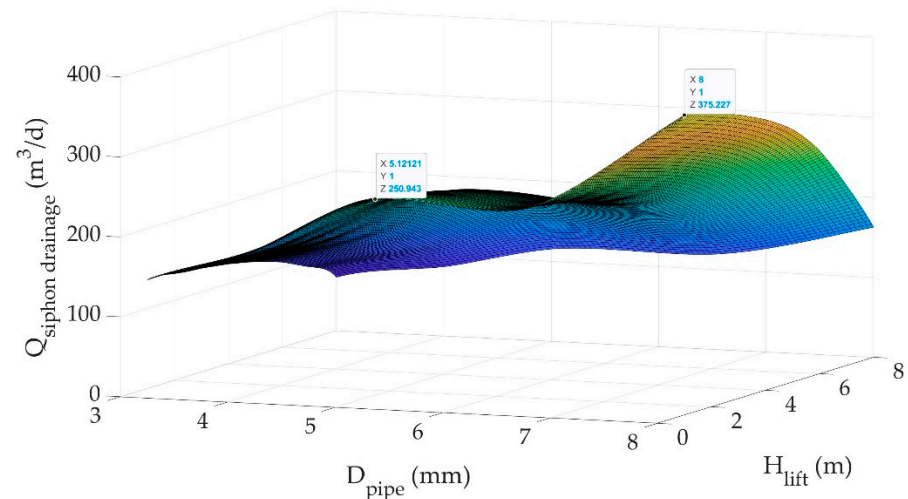
$$Q = vAt = 0.0216\pi d^2 v \left(\text{m}^3/\text{d} \right) \tag{8}$$

where t refers to the time of a day. Then, the single-day drainage capacity of multiple siphons in a borehole is

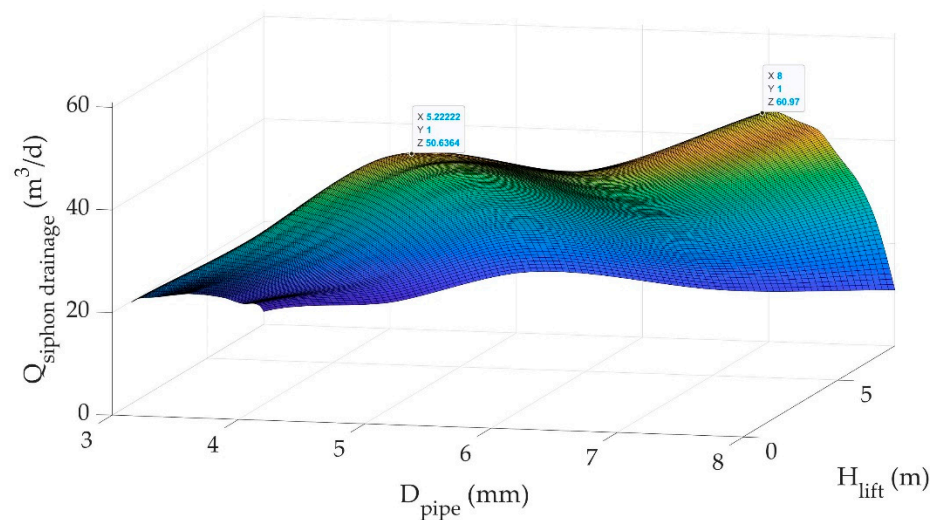
$$Q_{dmm} = nq_{dmm} = 0.0216\pi d^2 nv \tag{9}$$

Figure 13a,b shows surface fits of the drainage capacity for each pipe diameter at different lifts (x-axis—siphon diameter, y-axis—lift, z-axis—discharge) for 30 m and 200 m lengths of siphons, respectively. The siphon discharge capacity of a single short pipe strictly follows the rule “the larger the pipe diameter, the higher the discharge capacity,” but the number of siphons placed in the same size borehole is not proportional to the siphon diameter. The surface fit shows that the water-lowering capacity of the short siphon increases with the diameter of the pipe. It is worth noting that the D-6.5 and D-8 siphons do not have long-term application stability and only increase the surface fit’s reliability in the MATLAB iterative calculations and are not used as pipe diameters to be considered. Figure 13 shows that peak drainage occurs near the 5.2 mm position, which is determined by the product function of the total cross-sectional area of the siphons lined up in the borehole and the flow rate (i.e., the single-hole drainage). However, as the total length of the siphon increases, the positive relationship between drainage capacity and siphon

diameter gradually changes. D-5 siphons perform increasingly well and show a smaller decrease in drainage capacity with changes in pipe length and other factors compared to D-8 pipes. Therefore, the D-5 siphon performs best for all pipe diameters.



(a)



(b)

Figure 13. Drainage capacity under engineered piping conditions in 10 cm diameter boreholes: (a) siphon length 30 m; (b) siphon length 200 m.

Based on the factors influencing siphon drainage capacity described in the paper, the borehole diameter and siphon wall thickness are superficially more favorable to process improvement measures in terms of enhancing siphon drainage capacity. However, since the borehole and siphon are circular, the siphon placement problem can be reduced to a geometric problem of “small circles inside large circles”. According to this equation, the calculated number of placements is a non-exact result applicable to the construction conditions. According to the calculation principle, when the diameter of the borehole increases, the proportional increase in the number of construction placements for each pipe diameter is not unidirectional and linear and may even fluctuate. Therefore, the borehole size can be freely determined according to the project’s needs in the actual project.

5. Conclusions

Landslide disasters mainly occur in the rainy season, which is related to the softening of slope soils, reduced shear strength, and increased pore water pressure caused by the elevation of the groundwater level due to rainfall. Therefore, comprehensive disaster-causing factors and timely groundwater level reduction is the most direct and effective control method with low cost. Among the various methods of groundwater level reduction, the siphon drainage technique has distinct advantages because it requires no additional energy supply while its drainage capacity dynamically adjusts with water level changes. The research work obtained the following results and insights by comparing the performance of different pipe diameters concerning lift and length and restarting capacity through an original scale model.

1. The flow rate of siphon drainage is influenced by several factors, including pipe diameter, pipe length, and lift, of which pipe length and lift are both uncontrollable factors in practical engineering. Hence, optimizing siphon pipe diameter is the most direct and effective way to address the efficiency and permanence of siphon drainage systems.
2. The typical pipe diameters of siphons are categorized and discussed according to the proportional difference in the size of the gravitational and viscous force influence caused by the pipe diameter. Among them, 5 mm pipe diameter as a transition pipe diameter between capillary and typical pipe diameter, under different capillary number and Reynolds number conditions, both capillary action and gravitational action dominant dual characteristics, can form a stable slug flow while maintaining the existence of liquid film to prevent increased friction losses along the way.
3. In the lateral comparison of five pipe diameters in the same single hole surge capacity under the conditions of lowering water level capacity, an 8 mm siphon pipe for lowering of water level capacity for the maximum, yet poor long-term effectiveness was not considered. Moreover, carefully considering each pipe diameter drainage capacity and single borehole cloth pipe program, 5 mm pipe diameter siphon total drainage capacity was of good performance. The combined pipe diameter test and drainage requirements show that the 5 mm pipe diameter, as a demarcating pipe diameter with the advantages of both surface tension and gravity, can meet the higher drainage requirements while ensuring the timely discharge of accumulated gas by the flow pattern in the pipe, guaranteeing the long-term effectiveness of long-distance siphon drainage. The results of the study will provide inspiration for the selection of optimal pipe diameters for future engineering applications.

In future studies, the model performance of ultra-long tubes (siphon lengths greater than 200 m) will be further explored. In addition, the application of siphon drainage technology to different soil slopes or climatic conditions can also be a future research option.

Author Contributions: Conceptualization, formal analysis, H.S. and Y.S.; methodology, software, validation, investigation, resources, data curation, writing—original draft preparation, writing—review and editing, Y.Z. All authors have read and agreed to the published version of the manuscript.

Funding: This study was supported by the National Natural Science Foundation of China (42230702).

Institutional Review Board Statement: Not applicable.

Informed Consent Statement: Not applicable.

Data Availability Statement: Not applicable.

Conflicts of Interest: The authors declare no conflict of interest. The funders had no role in the design of the study, in the collection, analyses, or interpretation of data, in the writing of the manuscript, or in the decision to publish the results.

References

1. Bračko, T.; Žlender, B.; Jelušič, P. Implementation of Climate Change Effects on Slope Stability Analysis. *Appl. Sci.* **2022**, *12*, 8171. [[CrossRef](#)]
2. Gao, Y.; Yin, Y.; Li, B.; Feng, Z.; Wang, W.; Zhang, N.; Xing, A. Characteristics and Numerical Runout Modeling of the Heavy Rainfall-Induced Catastrophic Landslide–Debris Flow at Sanxicun, Dujiangyan, China, Following the Wenchuan Ms 8.0 Earthquake. *Landslides* **2017**, *14*, 1361–1374. [[CrossRef](#)]
3. Qu, M.; Dang, F. Numerical Analysis of Instability Mechanism of a High Slope under Excavation Unloading and Rainfall. *Appl. Sci.* **2022**, *12*, 7990. [[CrossRef](#)]
4. Chen, Y.Y.; Tang, H.M.; Zhou, Z.M. Optimization of Port Bank Slope Drainage Technique in Three Gorges Area. *Port Waterw. Eng.* **2006**, *5*, 50–54.
5. Hongyue, S.; Yuequan, S. *Slope Siphon Drainage Theory and Practice*, 1st ed.; China Science Publishing & Media: Beijing, China, 2016; pp. 12–156.
6. Sun, H.; Wang, D.; Shang, Y.; Cai, Y.; Wei, Z. An Improved Siphon Drainage Method for Slope Stabilization. *J. Mt. Sci.* **2019**, *16*, 701–713. [[CrossRef](#)]
7. Cai, Y.; Sun, H.; Shang, Y.; Xiong, X. An Investigation of Flow Characteristics in Slope Siphon Drains. *J. Zhejiang Univ. Sci. A* **2014**, *15*, 22–30. [[CrossRef](#)]
8. Mei, C.; Liang, X.; Sun, H.; Wu, M. High-Lift Siphon Flow Velocity in a 4-Mm Siphon Hose. *J. Zhejiang Univ. Sci. A* **2017**, *18*, 487–495. [[CrossRef](#)]
9. Yu, Y.; Shen, M.; Sun, H.; Shang, Y. Robust Design of Siphon Drainage Method for Stabilizing Rainfall-Induced Landslides. *Eng. Geol.* **2019**, *249*, 186–197. [[CrossRef](#)]
10. Tohari, A.; Wibawa, S.; Koizumi, K.; Oda, K.; Komatsu, M. Effectiveness of Siphon Drainage Method for Landslide Stabilization in a Tropical Volcanic Hillslope: A Case Study of Cibitung Landslide, West Java, Indonesia. *Bull. Eng. Geol. Environ.* **2021**, *80*, 2101–2116. [[CrossRef](#)]
11. Hongyue, S.; Pan, P.; Qing, L. A case study of a rainfall-induced landslide involving weak interlayer and its treatment using the siphon drainage method. *Bull. Eng. Geol. Environ.* **2019**, *78*, 4063–4074.
12. Waskito, K.T.; Pratama, S.Y.; Candra, B.D.; Rahmat, B.A. Comparison of Microbubble and Air Layer Injection with Porous Media for Drag Reduction on a Self-Propelled Barge Ship Model. *J. Mar. Sci. Appl.* **2018**, *17*, 165–172.
13. Blake, T.D. The Physics of Moving Wetting Lines. *J. Colloid Interface Sci.* **2006**, *299*, 1–13. [[CrossRef](#)] [[PubMed](#)]
14. Blake, T.D.; Bracke, M.; Shikhmurzaev, Y.D. Experimental Evidence of Nonlocal Hydrodynamic Influence on the Dynamic Contact Angle. *Phys. Fluids* **1999**, *11*, 1995–2007. [[CrossRef](#)]
15. Barnea, D.; Luninski, Y.; Taitel, Y. Flow Pattern in Horizontal and Vertical Two Phase Flow in Small Diameter Pipes. *Can. J. Chem. Eng.* **1983**, *61*, 617–620. [[CrossRef](#)]
16. Mandhane, J.M.; Gregory, G.A.; Aziz, K. A Flow Pattern Map for Gas–Liquid Flow in Horizontal Pipes. *Int. J. Multiph. Flow* **1974**, *1*, 537–553. [[CrossRef](#)]
17. Lee, C.Y.; Lee, S.Y. Pressure Drop of Two-Phase Dry-Plug Flow in Round Mini-Channels: Effect of Moving Contact Line. *Exp. Therm. Fluid Sci.* **2010**, *34*, 1–9. [[CrossRef](#)]
18. Yu, D.; Choi, C.; Kim, M.H. Pressure Drop and Dynamic Contact Angle of Triple-Line Motion in a Hydrophobic Microchannel. *Exp. Therm. Fluid Sci.* **2012**, *39*, 60–70. [[CrossRef](#)]
19. Park, S.C.; Kwak, H.J.; Kim, M.H.; Fezzaa, K.; Lee, Y.W.; Yu, D.I. Pressure Drop with Moving Contact Lines and Dynamic Contact Angles in a Hydrophobic Round Minichannel: Visualization via Synchrotron X-Ray Imaging and Verification of Experimental Correlations. *Langmuir* **2020**, *36*, 11207–11214. [[CrossRef](#)]
20. Klaseboer, E.; Gupta, R.; Manica, R. An Extended Bretherton Model for Long Taylor Bubbles at Moderate Capillary Numbers. *Phys. Fluids* **2014**, *26*, 032107. [[CrossRef](#)]
21. Brauner, N.; Maron, D.M. Identification of the Range of ‘Small Diameters’ Conduits, Regarding Two-Phase Flow Pattern Transitions. *Int. Commun. Heat Mass Transf.* **1992**, *19*, 29–39. [[CrossRef](#)]
22. Angeli, P.; Gavriilidis, A. Hydrodynamics of Taylor Flow in Small Channels: A Review. *Proc. Inst. Mech. Eng. Part C J. Mech. Eng. Sci.* **2008**, *222*, 737–751. [[CrossRef](#)]
23. Mengping, W.; Hongyue, S. Slope siphon drainage hole spacing study. *J. Nat. Disasters* **2017**, *26*, 40–46.